

A maximum likelihood approach to the destriping technique

¹ University of Helsinki, Department of Physical Sciences, P.O. Box 64, FIN-00014, Helsinki, Finland

² Helsinki Institute of Physics, P.O. Box 64, FIN-00014, Helsinki, Finland

³ Dipartimento di Fisica, Università di Milano, Via Celoria 16, I-20131, Milano, Italy

⁴ IASF/CNR, Sezione di Bologna, Via Gobetti 101, I-40129, Bologna, Italy

Sent, 23 April 2003

Abstract. The destriping technique is a viable tool for removing different kinds of systematic effects in CMB related experiments. It has already been proven to work for gain instabilities that produce the so-called $1/f$ noise and periodic fluctuations due to e.g. thermal instability. Both effects when coupled with the observing strategy result in stripes on the observed sky region. Here we present a maximum-likelihood approach to this type of technique and provide also a useful generalization. As a working case we consider a data set similar to what the PLANCK satellite will produce in its Low Frequency Instrument (LFI). We compare our method to those presented in the literature and find some improvement in performance. Our approach is also more general and allows for different base functions to be used when fitting the systematic effect under consideration. We study the effect of increasing the number of these base functions on the quality of signal cleaning and reconstruction. This study is related to PLANCK LFI activities.

Key words. methods: data analysis – cosmology: cosmic microwave background

1. Introduction

One of the major goals for cosmology is to determine the cosmological parameters which describe the structure and evolution of the Universe. In this respect CMB observations are a powerful tool probing directly the early phases of the Universe. Recent results from the WMAP satellite (Bennett et al. 2003) show that high accuracy in such measurements can be achieved with an optimal choice of observing site (the second Lagrange point of the Sun-Earth system, L_2 , for good thermal and environmental stability), careful instrument design and control of systematic effects. The latter is related to the observing strategy adopted, which should be as redundant as possible, with different measurements of the same sky region with different detectors and on different time scales in order to properly control systematics.

Future space missions like PLANCK¹ which are designed to have a signal-to-noise ratio of the order of few tens (far larger than WMAP), require control of systematic effects at the μK level. In this respect several techniques have been developed to treat systematics, detect and remove them in the best possible way. Burigana et al. (1997), Delabrouille (1998), and Maino et al. (1999, 2002)

have considered, in the context of the PLANCK mission, a simple destriping algorithm to remove systematics like the $1/f^\alpha$ noise. Mennella et al. (2002) have instead considered destriping when dealing with periodic fluctuations as those induced by thermal instabilities.

Destriping methods work on time-ordered data (TOD) and produce TOD cleaned from systematics. When TOD is cleaned it is possible to coadd observations on the same region (pixel) of the sky to obtain a sky map which gives a visual impression of the data. Though it is non-optimal, in the sense that it would not necessarily produce the map with the minimum possible variance as instead provided by the Generalized Least Square solution of the map-making problem (see e.g. Natoli et al. 2001), it provides a fast and accurate map-making algorithm.

In this paper we consider the destriping technique in the light of maximum-likelihood analysis and present a general formulation of the destriping technique. We restrict our analysis to $1/f$ noise fluctuations. They produce noise which is strongly correlated in time and, when coupled with the observing strategy, will lead to stripes in the final maps that would alter the signal statistics. This is of extreme importance for the CMB which is expected to be a Gaussian random field.

The basic idea in destriping is to model the noise in the TOD by a linear combination of simple arithmetic functions, such as polynomials or Fourier components. The

Send offprint requests to: H. Kurki-Suonio, e-mail: hannu.kurki-suonio@helsinki.fi

¹ <http://astro.estec.esa.nl/SA-general/Projects/Planck/>

amplitudes of these base functions are determined taking advantage of the redundancy of the scanning strategy for which the same points on the sky are monitored several times during the mission. In its simplest form destriping involves fitting uniform baselines, i.e. one baseline for each elementary scanning period. In order to improve the accuracy of the method, we present here the possibility of fitting several components (base functions).

The destriping method of Burigana et al. (1997) and Maino et al. (1999, 2002) differs from the destriping method of Delabrouille (1998) in the weights they assign to different map pixels based on the number of measurements falling on that pixel. Our maximum-likelihood analysis presented in this paper leads to a weighting scheme that differs from both of these. Therefore we compare results obtained from all these three methods.

The paper is organized as follows. In Sect. 2 we present the maximum-likelihood approach to the destriping technique, Sect. 3 presents the main results, while we draw our conclusions in Sect. 4.

2. Destriping – maximum likelihood approach

2.1. General theory

In the following we present a maximum-likelihood based approach to the general destriping problem. We assume that data produced by a generic detector at a given time t could be written as:

$$y_t = P_{tp}m_p + n_{t,\text{corr}} + n_t \quad (1)$$

where m_p is the sky signal, assumed to be pixelized, P_{tp} is the pointing matrix, p is the pixel index, $n_{t,\text{corr}}$ is the correlated noise component while n_t is the white noise component. The variance of the white noise component is represented by a diagonal matrix \mathbf{C}_n in the time domain. Eq.(1) could be written in vector form as:

$$\mathbf{y} = \mathbf{P}\mathbf{m} + \mathbf{n}_{\text{corr}} + \mathbf{n}. \quad (2)$$

The exact properties of the matrix P , that spreads the map \mathbf{m} into TOD will be discussed in Sect. 2.2.

We model the correlated noise component of the TOD as a linear combination of a set of base functions (e.g. Fourier components, Legendre polynomials) as $\mathbf{n}_{\text{corr}} = \mathbf{F}\mathbf{a}$. Here F is a matrix, whose columns contain the base functions, and \mathbf{a} is a vector containing the (unknown) amplitudes of these base functions. It is convenient to select an orthogonal set of the base functions, so that $F^T F$ is diagonal.

With these assumptions, we obtain the likelihood function

$$\begin{aligned} \chi^2 &= \mathbf{n}^T \mathbf{C}_n^{-1} \mathbf{n} + \mathbf{a}^T \mathbf{C}_a^{-1} \mathbf{a} \\ &= (\mathbf{y} - \mathbf{F}\mathbf{a} - \mathbf{P}\mathbf{m})^T \mathbf{C}_n^{-1} (\mathbf{y} - \mathbf{F}\mathbf{a} - \mathbf{P}\mathbf{m}) \\ &\quad + \mathbf{a}^T \mathbf{C}_a^{-1} \mathbf{a}. \end{aligned} \quad (3)$$

Here the matrix \mathbf{C}_a represents the *a priori* covariance of the amplitudes \mathbf{a} .

If N_t is the length (the number of samples) of the TOD stream, N_{pix} is the number of pixels in the map, and N_a is the number of unknown amplitudes, then the sizes of the matrices are: $[F] = (N_t, N_a)$, $[P] = (N_t, N_{\text{pix}})$, $[\mathbf{C}_n] = (N_t, N_t)$ and $[\mathbf{C}_a] = (N_a, N_a)$.

We now want to find the maximum likelihood solution for \mathbf{a} . We need to minimize the function in Eq. (3) with respect to both of the unknown variables \mathbf{m} and \mathbf{a} .

First we find the minimum with respect to \mathbf{m} ,

$$\nabla_{\mathbf{m}} \chi^2 = -2\mathbf{P}^T \mathbf{C}_n^{-1} (\mathbf{y} - \mathbf{F}\mathbf{a} - \mathbf{P}\mathbf{m}) = 0. \quad (4)$$

From this we can solve the map \mathbf{m} using the fact that \mathbf{C}_n is diagonal,

$$\mathbf{m} = (\mathbf{P}^T \mathbf{P})^{-1} \mathbf{P}^T (\mathbf{y} - \mathbf{F}\mathbf{a}). \quad (5)$$

Substituting Eq. (5) back into Eq. (3) we obtain

$$\chi^2 = \chi_n^2 + \chi_a^2, \quad (6)$$

where

$$\chi_n^2 = (\mathbf{y} - \mathbf{F}\mathbf{a})^T \mathbf{Z} (\mathbf{y} - \mathbf{F}\mathbf{a}) / \sigma^2, \quad (7)$$

$$\chi_a^2 = \mathbf{a}^T \mathbf{C}_a^{-1} \mathbf{a}, \quad (8)$$

and

$$\mathbf{Z} = \mathbf{I} - \mathbf{P}(\mathbf{P}^T \mathbf{P})^{-1} \mathbf{P}^T. \quad (9)$$

Here \mathbf{I} denotes the unit matrix, and the property $\mathbf{Z}^T \mathbf{Z} = \mathbf{Z}$ has been used.

The next step is to minimize χ^2 with respect to \mathbf{a} ,

$$\nabla_{\mathbf{a}} \chi^2 = -2\mathbf{F}^T \mathbf{Z} (\mathbf{y} - \mathbf{F}\mathbf{a}) / \sigma^2 + 2\mathbf{C}_a^{-1} \mathbf{a} = 0, \quad (10)$$

which gives

$$\mathbf{a} = [\mathbf{F}^T \mathbf{Z} \mathbf{F} + \sigma^2 \mathbf{C}_a^{-1}]^{-1} \mathbf{F}^T \mathbf{Z} \mathbf{y}. \quad (11)$$

The matrix \mathbf{C}_a represents *a priori* information on the vector \mathbf{a} . If we do not have information on the noise properties (or we do not want to use any), the most simple choice is $\sigma^2 \mathbf{C}_a^{-1} = \mathbf{I}$. (Note that we cannot choose $\sigma^2 \mathbf{C}_a^{-1} = 0$, because matrix $\mathbf{F}^T \mathbf{Z} \mathbf{F}$ in general is singular.) This means ignoring the correlations between the elements of \mathbf{a} and assuming equal variance for all of them. Moreover, this means taking the variance to be the same for \mathbf{a} as for the white noise \mathbf{n} . There is, of course, no reason why this should hold true for the real noise, but in this way the variance cancels out from the equations, and we obtain a method which requires no input about the noise properties.

In what follows we thus assume $\mathbf{C}_a = \sigma^2$, using the same σ for \mathbf{C}_a and \mathbf{C}_n . The general case with $\mathbf{C}_a \neq \sigma^2$ will be treated in a subsequent paper.

To summarize, the maximum likelihood solution to the amplitude vector is

$$\mathbf{a} = [\mathbf{F}^T \mathbf{Z} \mathbf{F} + \mathbf{I}]^{-1} \mathbf{F}^T \mathbf{Z} \mathbf{y}, \quad (12)$$

where

$$\mathbf{Z} = \mathbf{I} - \mathbf{P}(\mathbf{P}^T \mathbf{P})^{-1} \mathbf{P}^T. \quad (13)$$

When the amplitude vector \mathbf{a} has been determined, the CMB map can be computed according to Eq. (5). These equations are the main theoretical result of this paper.

2.2. Pointing and beam shape

In the previous section we made no assumptions on the beam shape or on the pointing matrix \mathbf{P} . In principle, the beam shape and profile can be incorporated in \mathbf{P} . The elements of \mathbf{P} then determine the weights that different pixels contribute to a given measurement. This way beams with arbitrary shapes and profiles can be treated. In this case the matrix $\mathbf{P}^T \mathbf{P}$ is non-diagonal. Due to its large size in PLANCK type of missions its inversion would present a major computational burden.

A simpler approach is to consider each sample in the TOD to represent the temperature of the pixel at the center of the beam. Then \mathbf{P} takes a particularly simple form, consisting of ones and zeros for a full-power measurement like PLANCK. Each row contains one non-zero element identifying the pixel on which the corresponding measurement falls. Matrix $\mathbf{P}^T \mathbf{P}$ becomes diagonal, the diagonal elements giving the number of hits on each pixel. We follow this approach from here on.

In our simulations we have assumed a symmetric gaussian beam, and convolved the input map with the beam.

We mention here yet another possibility of interpreting the pointing matrix. Instead of a pixelized map, the vector \mathbf{m} could be interpreted as the set of multipoles $a_{\ell m}$ which determine the sky signal, in the spirit of harmonic analysis (Challinor et al. 2002). Matrix \mathbf{P} then consists of the values of the spherical harmonics at measurement directions, possibly combined with beam weights in the case of non-symmetric beam. We do not pursue this idea further here, but we note that the formalism presented in Sect. 2.1 applies to any situation where the sky temperature is represented by a linear function \mathbf{Pm} , as long as matrix $\mathbf{P}^T \mathbf{P}$ is non-singular.

2.3. Circular scanning

In the nominal scanning strategy of PLANCK the spin axis follows the ecliptic plane. The spin axis is kept anti-solar by repointing it by $2.5'$ every hour. The spacecraft rotates around the spin axis at a rate of 1 rpm. During one hour PLANCK scans the same circle on the sky 60 times. As the sky signal is almost time-independent, the data can be coadded to reduce the length of the data stream by a factor of 60. We call this set of 60 circles, and the corresponding segment of the coadded TOD a ‘‘ring’’. The crossing points of the rings are important calibration points, which allow for the removal of the correlated noise component from the TOD.

The opening angle of the scanning circle varies between 80-90 degrees, depending on the location of the detector on the focal plane. The sampling frequency for the 100 GHz LFI receiver is 108.3 Hz. The instrument then collects 6498 temperature values, or ‘‘samples’’, at each rotation of the spacecraft, corresponding roughly to a $3'$ shift between successive samples. A total of 8766 rings builds up one year of observations.

In reality, the angular velocity of the rotation does not stay exactly constant, especially immediately after repointing, and the samples from different circles of the same ring are shifted in position. This will probably require discarding the first few circles of each ring, and resampling or phase binning the rest before performing the coaddition. During the ring the spin axis of the satellite will follow a nutation ellipse with maximum amplitude of $1.5'$ at the end of the nutation damping phase (van Leeuwen et al. 2002). This may degrade slightly the performance of destriping. We ignore these complications in this paper.

The destriping technique applies particularly well to a PLANCK-like measurement pattern resulting from the coadding of scanning circles into rings which breaks the stationarity of the data. The $1/f^\alpha$ noise component in the coadded TOD is well presented by a piecewise defined function, where each piece consists of a linear combination of a few base functions.

As shown by Delabrouille (1998) and Maino et al. (1999, 2002), a simple model with uniform baselines and white noise models quite well the coadded noise stream. One can try to further improve the performance of destriping by introducing more base functions. Delabrouille (1998) found that the addition of a small number of base functions improved the performance of destriping, whereas Maino et al. (2002) found no significant improvement. The difference between these results could be due to the different noise spectra considered: $1/f$ noise for Maino et al. (2002) and $1/f^2$ for Delabrouille (1998).

2.4. Base functions

We have studied two sets of base functions: Fourier components and Legendre polynomials. Both form an orthogonal set.

We return now to the formalism introduced in Sect. 2.1. Matrix \mathbf{F} obtains the form $F_{ik,jq} = f_{qk} \delta_{ij}$, where $k = 0, \dots, n_{\text{samp}} - 1$ labels samples on a scanning ring, $q = 0, \dots, Q - 1$ labels the base functions, and i, j label rings. The combined index ik identifies a data point (a ‘‘measurement’’) in the coadded TOD. Similarly, index jq identifies an element in vector \mathbf{a} . Matrix f_{qk} gives the component functions. For instance in the case of Fourier modes, $f_{qk} = \cos(q\pi k/n_{\text{samp}})$ for $q = 0, 2, 4, \dots$ and $f_{qk} = \sin((q+1)\pi k/n_{\text{samp}})$ for $q = 1, 3, \dots$. In the second case we have $f_{qk} = L((2k+1)/n_{\text{samp}} - 1, q)$, where $L(x, n)$ is the n th Legendre polynomial. In both cases $q = 0$ gives the uniform baseline.

2.5. Comparison with earlier work

In this section we consider the special case where the base functions include uniform baselines only ($Q = 1$). We assume the pointing matrix is of the simple form explained in Sect. 2.2. Without changing the minimization of χ^2 we

can set $\sigma = 1$. With these assumptions Eqs. (7) and (8) become

$$\chi_n^2 = \sum_p \frac{\sum_{ik,jl} (a_i - a_j - y_{ik} + y_{jl})^2 d_{ik}^p d_{jl}^p}{2 \sum_{ik} d_{ik}^p} \quad (14)$$

and

$$\chi_a^2 = \sum_i a_i^2, \quad (15)$$

where index p labels pixels, i, j scanning rings, and k, l samples on a given ring. A combined index ik or jl identifies a measurement. We define the symbol d_{ik}^p so that $d_{ik}^p = 1$ if measurement ik falls into pixel p , otherwise $d_{ik}^p = 0$. Due to the factors d_{ik}^p and d_{jl}^p in the numerator of Eq. (14) only those pixels p contribute to the pixel sum which lie on two or more scanning rings, and the sum $\sum_{ik,jl}$ is equal to 2 times the sum over all *pairs* of measurements falling on pixel p .

Eqs. (14) and (15) can be compared to Eq. (2) of Maino et al. (1999) or to Eq. (10) of Burigana et al. (1997). The formulas differ in that in Eq. (14) χ^2_n has in the denominator the term $n_p = \sum_{ik} d_{ik}^p$, which gives the total number of hits in pixel p . Secondly, instead of the χ^2_a of Eq. (15), Maino et al. (1999) and Burigana et al. (1997) have

$$\chi_a^{2'} = \left(\sum_i a_i \right)^2, \quad (16)$$

which is equivalent to choosing $\mathbf{C}_a^{-1}\sigma^2 = \mathbf{1}\mathbf{1}^T$, where $\mathbf{1}\mathbf{1}^T$ denotes a matrix with all elements equal to one.

Delabrouille (1998) gives the general form

$$S = \sum_{p \in \text{sky pairs}} \sum w(p, ik, jl) (y_{ik} - y_{jl} - a_i + a_j)^2 \quad (17)$$

for the function S to be minimized. Here the second sum refers to all pairs (ik, jl) that can be formed of the measurements falling into pixel p , and w is a weight function to be chosen. Based on the fact that pixel p contributes $n_p(n_p - 1)/2$ pairs, Delabrouille suggests choosing $w \propto 1/(n_p - 1)$. The result of Maino et al. (1999) corresponds to $w = \text{const.}$ and our new result, Eq. (14) to $w = 1/n_p$.

The term χ_a^2 has the important function of removing the degeneracy involved in the minimization of χ_n^2 . It is clear from looking at Eq. (14), that the minimum of χ_n^2 is not unique. One can add a constant to all components a_i without changing the value of χ_n^2 .

While Eq. (15) arises from a probabilistic theory, Eq. (16) was introduced as a technical term designed to remove the degeneracy mentioned, and to force $\sum_i a_i = 0$. We show in Sect. 3, that in practice the difference between these two approaches is small. However, it is not evident how Eq. (16) generalizes to the case of several base functions, which may bring about new degeneracies.

3. Simulation results

3.1. Data set

We have carried out simulations of the Planck LFI 100 GHz detector. The underlying CMB map was created by the Synfast code of the HEALPix package², starting from the CMB anisotropy angular power spectrum computed with the CMBFAST code³ using the cosmological parameters $\Omega_{\text{tot}} = 1.00$, $\Omega_{\Lambda} = 0.7$, $\Omega_{\text{b}}h^2 = 0.02$, $h = 0.7$, $n = 1.00$, and $\tau = 0.0$. We created the input map with HEALPix resolution $N_{\text{side}} = 1024$ and with symmetric Gaussian beam with full width at half maximum (FWHM) of $10'$. We then formed the signal TOD by picking temperatures from this map. All our output maps have resolution parameter $N_{\text{side}} = 512$, corresponding to angular resolution $7'$.

The scanning pattern corresponds to the nominal PLANCK scanning strategy of the 100 GHz LFI detector number 10.⁴ The angle between the satellite spin axis and the optical axis of the telescope is 85°. The beam center is pointing towards $(\theta, \phi) = (3^\circ 737, 126^\circ 228)$. Here θ is the angle from the optical axis and ϕ is an angle counted clockwise from the axis pointing from the center of the focal plane towards the satellite spin axis. We assumed no spin axis precession. Our simulated data set consists of 5040 scanning rings, corresponding to 7 months of measurement time. The TOD stream contains 6498 samples on each ring, corresponding to a sampling frequency of $f_s = 108.3$ Hz. The sky coverage is 98.5%.

The rings cross at points which are mostly concentrated near the ecliptic poles. We count as crossing points all points where two measurements on different rings fall on the same pixel. Since our pixel resolution ($7'$) exceeds the repointing angle of the spin axis ($2.5'$), the crossing points include cases where two nearby rings pass parallel through the same pixel, without actually crossing each other.

We used the Stochastic Differential Equation (SDE) technique to create the instrument noise stream, which we added to the signal TOD.⁵ We generated noise with power spectrum

$$P(f) = \left(1 + \frac{f_k}{f}\right) \frac{\sigma^2}{f_s}, \quad (f > f_{\min}) \quad (18)$$

with parameters $\sigma = 4800\mu\text{K}$ (CMB temperature scale), $f_k = 0.1\text{Hz}$, and $f_{\min} = 10^{-6}\text{Hz}$. The parameter f_k is called the knee frequency. The noise level $4800\mu\text{K}$ corresponds to the estimated white noise level of one 100GHz LFI detector.

² <http://www.eso.org/science/healpix>

³ <http://physics.nyu.edu/matiasz/CMBFAST/cmbfast.html>

⁴ Simulation Software is part of the Level S of the PLANCK DPCs and is available for PLANCK collaboration at <http://planck.mpa-garching.mpg.de>.

⁵ SDE is one of the two methods in the Planck Level S pipeline for producing simulated instrument noise. The method was implemented by B. Wandelt and K. Górski and modified by E. Keihänen.

There was no foreground included in the simulations presented in this paper, but we have also verified our destriping codes on simulated data sets with foreground. We found that the foreground has an insignificant impact on the baselines determined by the destriping, in agreement with the discussion in Maino et al. (2002). The quality of destriping is also almost independent of the impact of another class of instrumental systematic effects, main beam distortions and straylight, as the temperature differences at crossing pixels are dominated by the noise and only minimally affected by the spurious signals ($\approx \mu\text{K}$) introduced by optical distortions (see e.g. Burigana et al. 2001).

3.2. Destriping codes

We have run simulations with two distinct destriping codes. Code I (“classical destriping”) is essentially the same as the code presented in Burigana et al. (1997), with modifications that allow comparison of the different weight functions discussed in Sect. 2.5. Code I only allows fitting uniform baselines.

Code II (“generalized destriping code”) applies the formalism presented in Sect. 2.1. Due to a different formulation of the problem the code does not include an explicit weight function that could be compared to w in Code I. Code II allows fitting arbitrary base functions.

The solution of the destriping problem involves the solution of a large linear system of equations. Code I uses the Cholesky decomposition technique to solve the linear system. The rank of the matrix involved increases proportional to the number of base functions. The solution of the system by Cholesky decomposition quickly becomes unfeasible as the number of base functions increases. Code II uses the iterative conjugate gradient method (see, e.g., Press et al. 1992) for solution.

Both codes have been written in Fortran-90.

We have checked that in the case of uniform baselines and weight $w = 1/n_p$ the two codes give the same results.

The matrix formalism derived in Sect. 2.1 allows us to perform the destriping in a relatively small memory space in Code II. It is not necessary to store the whole matrix $\mathbf{A} \equiv \mathbf{F}^T \mathbf{Z} \mathbf{F} + \mathbf{I}$, which may be very large, especially in the case of several base functions. The conjugate gradient method only requires multiplication by matrix \mathbf{A} . That can easily be done algorithmically, without actually storing the full matrix at any one time.

3.3. Comparison of different weighting schemes

Figure 1 shows the input C_ℓ spectrum and the spectrum derived from the simulated TOD after destriping. Destriping was done by Code II, fitting uniform baselines only. We used the Anafast code of the HEALPix package to compute the C_ℓ spectrum of the destriped map. We subtracted from the derived spectrum an estimate of the noise level $C_{\text{noise}} = 0.197\mu\text{K}^2$ (estimated as the average of C_ℓ over $\ell = 980 \dots 1000$) and corrected the spectrum for the

beam shape convolution and pixel convolution. The shown angular spectrum is thus $\tilde{C}_\ell = (C_\ell - C_{\text{noise}})/(B_\ell^2 h_\ell^2)$, where $B_\ell = \exp(-\sigma_b^2 \ell(\ell+1)/2)$, with $\sigma_b = 10'/\sqrt{8 \ln(2)}$, is the beam convolution function corresponding to the assumed beam width of $10'$ (FWHM), and h_ℓ is the pixel convolution function (provided by HEALPix package).

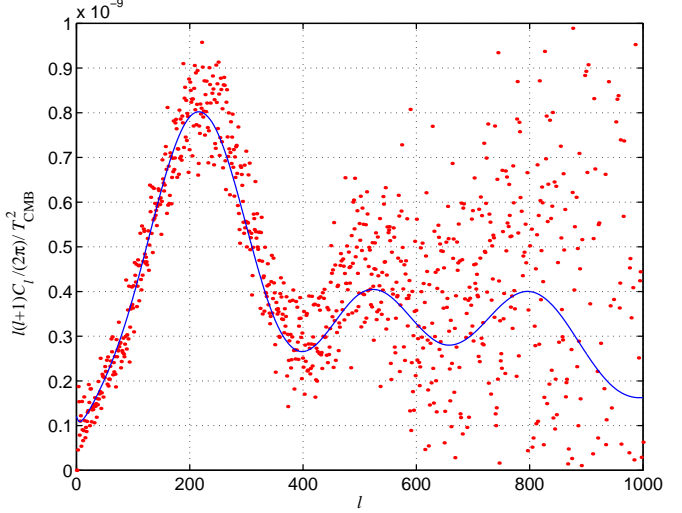


Fig. 1. The input C_ℓ spectrum and the spectrum computed from the CMB map. The latter has been corrected for beam and pixel convolution, and for white noise level. Destriping was done fitting uniform baselines only.

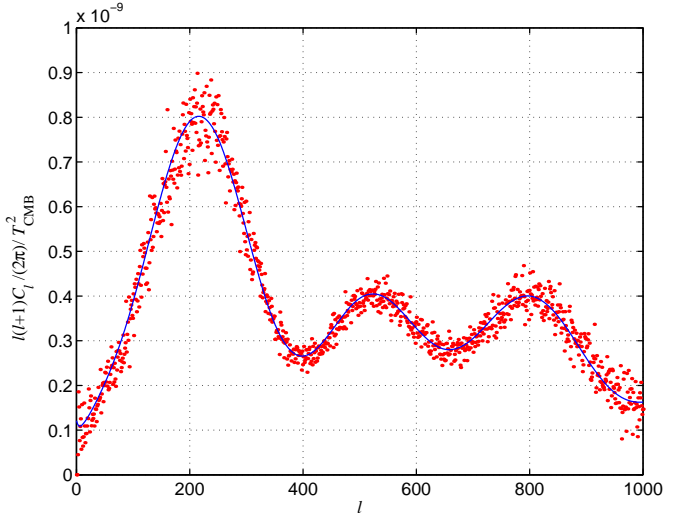


Fig. 2. Same as Fig. 1, but for noise level lowered by factor $1/\sqrt{24}$. This simulates the effect of combining 24 detectors.

Figure 2 shows the same for a noise level reduced by the factor $\sqrt{24}$, corresponding to the combination of 24 detectors. Here the subtracted noise level was $C_{\text{noise}} = 0.197\mu\text{K}^2/24 = 0.082\mu\text{K}^2$.

Note that Figs. 1 and 2 are for illustration only, as this paper does not address the full CMB C_ℓ estimation problem, and thus we have just used the above crude estimate for C_{noise} . The C_ℓ estimation problem will be addressed in a subsequent paper.

We have chosen the root-mean-square (rms) value of the residual noise map (see below) pixels as a figure of merit that we use to compare different destriping methods. This map rms is related to the C_ℓ spectrum through the relation

$$\text{rms}^2 = \sum_\ell \frac{2\ell + 1}{4\pi f_{\text{sky}}} C_\ell. \quad (19)$$

The map rms squared is thus a weighted sum of the angular spectrum, with high weight on high multipoles. The sky coverage $f_{\text{sky}} = 0.985$ enters here because we have computed our rms values over the visited pixels only. When computing C_ℓ spectra, we have set $T = 0$ in the remaining pixels.

We compute the residual noise map by taking the difference between the destriped map and the noise-free reference map and subtracting the monopole component. Note that because of the incomplete sky coverage, removing the monopole affects the C_ℓ spectrum at all ℓ (not only $\ell = 0$). The reference map is computed by coadding the pure signal TOD into a map of resolution $N_{\text{side}} = 512$. The expected contribution from white noise to the residual map rms is $220.95 \mu\text{K}$.

While the rms of the residual noise map is a natural measure of the CMB map quality, the main scientific interest is perhaps not in the CMB map itself, but rather in its angular power spectrum C_ℓ . It is therefore of interest to see the impact of the destriping methods on the different parts of the C_ℓ spectrum. The map rms is dominated by the high ℓ part, and does not reveal the difference in performance of the various methods in the low ℓ part. Thus we have computed the angular power spectra C_ℓ of the residual noise maps.

Because of the random nature of the noise, the result of a comparison between methods may vary from one noise realization to another. We therefore performed destriping 10 times, with different realizations of instrument noise. The underlying CMB map was kept the same. We then used the average of the 10 residual map rms values and the residual noise map C_ℓ spectra to compare the methods. We also calculated the standard deviation (std) of the 10 map rms and C_ℓ values, to see whether the differences between the methods were statistically significant.

Table 1 presents a comparison between different weight functions discussed in Sect. 2.5. The corresponding C_ℓ spectra are shown in Fig. 3. Weight functions $w = 1/n_p$ and $w = 1/(n_p - 1)$ in Eq. (17) give similar results, due to the fact that for most pixels $n_p \gg 1$. Weight $w = 1/n_p$ suggested by our maximum likelihood analysis is clearly superior to $w = 1$. However, the weight $w = 1/(n_p - 1)$ gives an even smaller rms, although the difference is very small. The difference of the rms between $w = 1$ and $w = 1/n_p$ is significant because the difference is about 10

times larger than the respective std of the rms. Although the difference between $w = 1/n_p$ and $w = 1/(n_p - 1)$ is less than the std between different noise realizations, it was in the same direction in each realization. The comparison was done using Code I and fitting uniform baselines only.

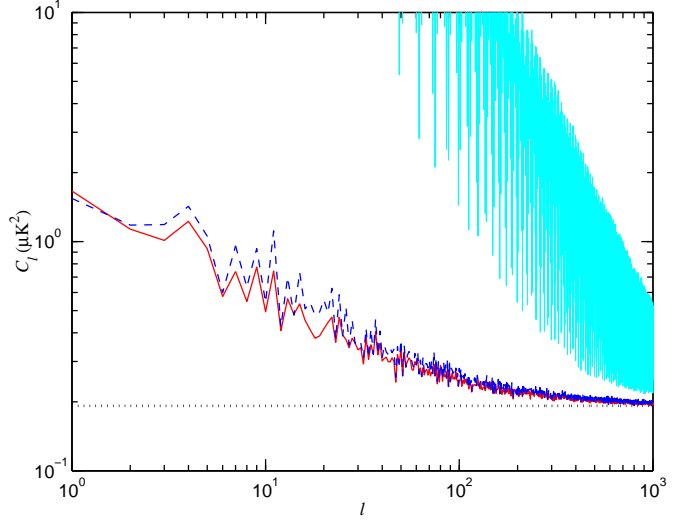


Fig. 3. The C_ℓ spectrum of the residual noise map, for different choices of the weight function w . Only constant baselines were included. The lower *solid* (red) line corresponds to the choice $w = 1/n_p$ for the weight function in Eq. (17) and the *dashed* (blue) line to $w = \text{const}$. The difference between weight functions $w = 1/n_p$ and $w = 1/(n_p - 1)$ is too small to show on this plot. The difference between them is plotted in Fig. 4 (lower panel). The upper *solid* (cyan) line shows the spectrum of a naive coadded map (no destriping). The corresponding map rms values are shown in Table I. The spectra were averaged over 10 realizations of noise. The *dotted* (black) line shows the theoretical white noise level $0.192 \mu\text{K}^2$.

Since the difference between the weight functions $w = 1/n_p$ and $w = 1/(n_p - 1)$ is so small that it does not show up in Fig. 3, we show just the differences in Fig. 4.

In Table 1 we compare also the two formulas, Eqs. (15) and (16), for χ_a^2 . The difference between the two is insignificant.

The scatter in the individual residual noise map C_ℓ values from one noise realization to another was larger than the difference between the methods. (See Fig. 5 for the C_ℓ spectra from the first three noise realizations, using our weighting scheme, $w = 1/n_p$.) The difference between $w = 1$ and $w = 1/n_p$ becomes however statistically significant when the C_ℓ are binned into larger bins.

Maximum-likelihood analysis is supposed to provide the minimum-variance solution. Therefore it may at first seem surprising that the maximum-likelihood based weight function did not give the best results. However, maximum-likelihood solution is the optimal one only if the model used corresponds to reality. Here we have modelled the $1/f$ noise component in the TOD by a uniform

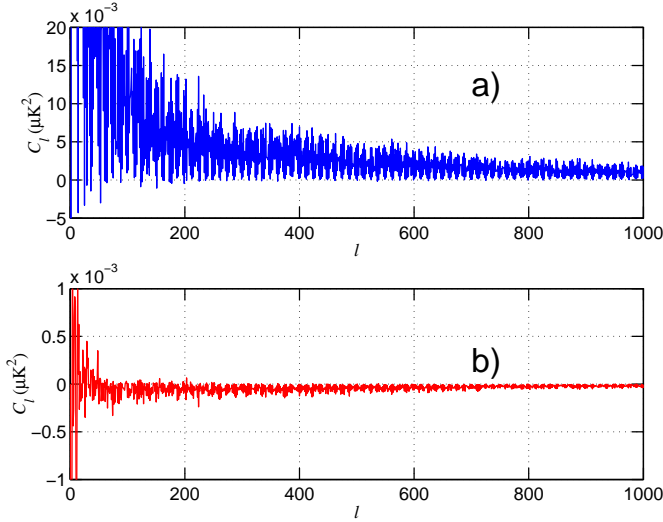


Fig. 4. Differences between the C_ℓ spectra shown in Fig. 3. **a)** The difference $C_\ell(w = \text{const}) - C_\ell(w = 1/n_p)$. **b)** The difference $C_\ell(w = 1/(n_p - 1)) - C_\ell(w = 1/n_p)$. Note the much expanded vertical scale in Fig. 4b.

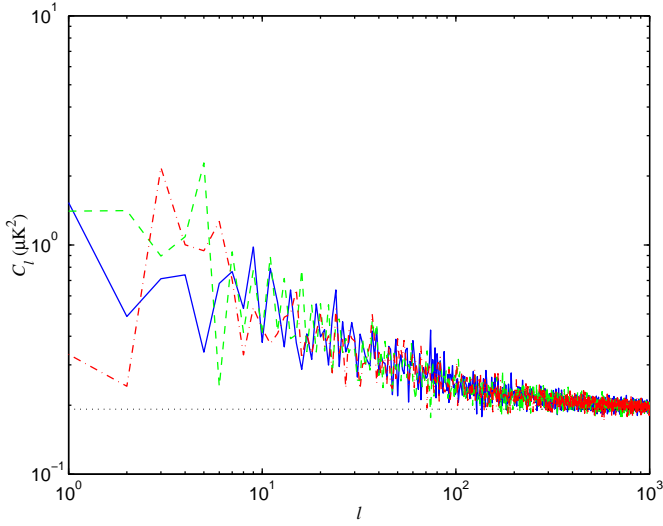


Fig. 5. Three examples of individual C_ℓ spectra, from different noise realizations, after destriping. Only uniform baselines are fitted. The average of 10 such spectra is shown in Fig. 6 (the bottom curve there).

baseline, which is a simplified model. Further, we have assumed that the baselines are independent from ring to ring. The reason for the maximum-likelihood solution not giving the best result is that the noise model used in the analysis does not exactly correspond to the actual noise properties.

To verify this, we re-generated our input noise in a way that better corresponds to the model assumed in the analysis. We generated the $1/f$ noise in the usual way, but then, for each ring, we took the average over the ring, and replaced the original $1/f$ contribution to the ring with this average value, on top of which we added white noise. This way we obtained noise which still has a realistic correla-

Table 1. Average (avg) rms and std of rms of the residual noise map for different weight functions. The average and std are taken over 10 noise realizations. Only uniform baselines were fitted. We compare also two formulas for χ^2 , A: Eq. (15), B: Eq. (16). The C_ℓ spectra corresponding to case A are shown in Fig. 3.

Weight	avg rms/ μK (A)	avg rms/ μK (B)
$w = 1$	225.16199	225.16202
$w = 1/(n_p - 1)$	224.43352	224.43350
$w = 1/n_p$	224.44466	224.44461
Weight	std of rms/ μK (A)	std of rms/ μK (B)
$w = 1$	0.07236	0.07237
$w = 1/(n_p - 1)$	0.07309	0.07369
$w = 1/n_p$	0.07313	0.07374

Table 2. Average rms and std of rms of the residual noise map, for a simplified noise model. Only uniform baselines were fitted. The noise consists of uniform baselines + white noise.

Weight	avg rms/ μK	std of rms/ μK
$w = 1$	221.48154	0.06911
$w = 1/(n_p - 1)$	221.10510	0.07144
$w = 1/n_p$	221.10493	0.07141

tion between scanning rings, but consists of baselines + white noise only. The results are shown in Table 2. Now the maximum-likelihood based weight function gives the smallest variance map.

Thus it seems that the slightly better performance of the Delabrouille weighting scheme ($w = 1/(n_p - 1)$) is related to the effect of that part of the correlated noise which deviates from uniform baselines.

3.4. Increasing the number of base functions

Table 3 and Figs. 6–10 present results of fitting several base functions using Code II. We compare four sets of functions:

1. (“Un.”) Uniform baselines only.
2. (“F1”) Uniform baseline + first Fourier frequency, which gives three components: constant, $\sin(2\pi f_{\text{sc}} t)$, and $\cos(2\pi f_{\text{sc}} t)$ ($q = 0, 1, 2$). Here $f_{\text{sc}} = 1/(60 \text{ s})$ is the scanning frequency.
3. (“L1”) Uniform baseline + 1st (linear) Legendre polynomial.
4. (“L2”) Uniform baseline + 1st and 2nd Legendre polynomials.

The first Legendre polynomials are $L(x, 0) = 1$, $L(x, 1) = x$, and $L(x, 2) = \frac{1}{2}(3x^2 - 1)$, for $x \in [-1, 1]$.

Again we averaged the residual noise C_ℓ spectra and the residual noise map rms over 10 noise realizations.

In order to check how the results depend on the knee frequency, we repeated our computations with rescaled noise. We took the $1/f$ noise stream, which was originally generated with $f_k = 0.1 \text{ Hz}$, scaled it by a factor 0.5 or 2, and added white noise with same variance in all cases.

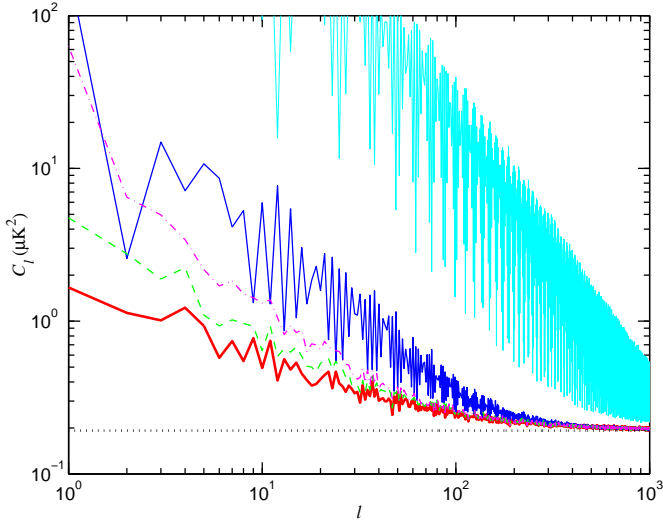


Fig. 6. Average C_ℓ spectrum of the residual noise map, for different choices of the base functions. *Thick solid* (red) line: uniform baselines. *Thin solid* (blue) lower line: three Fourier components ($q = 0, 1, 2$). *Dashed* (green) and *dot-dashed* (magenta) lines: Legendre polynomials up to 1st and 2nd order. The corresponding map rms values are shown in Table 3 in the middle column ($f_k = 0.1\text{Hz}$). The upper *solid* (cyan) line shows the spectrum of a naive coadded map (no destriping). The spectra were averaged over 10 realizations of noise.

This is equivalent to changing the knee frequency by a factor of 0.25 or 4. We thus have results for three knee frequencies: $f_k = 0.025\text{Hz}$, $f_k = 0.1\text{Hz}$, and $f_k = 0.4\text{Hz}$.

The obtained residual map rms are shown in Table 3. The C_ℓ spectra for the case $f_k = 0.1\text{Hz}$ are shown in Fig. 6, and the other two cases in Fig. 7 and Fig. 8. The std of the C_ℓ for the $f_k = 0.1\text{Hz}$ case are shown in Fig. 10.

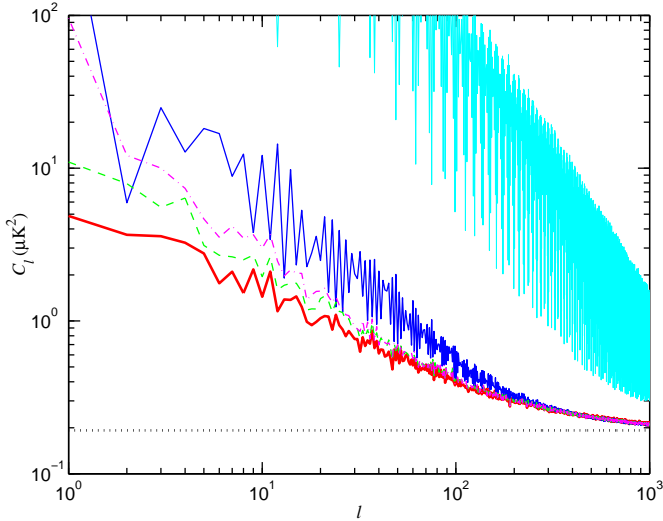


Fig. 7. Same as Fig. 6 but for knee frequency $f_k = 0.4\text{Hz}$.

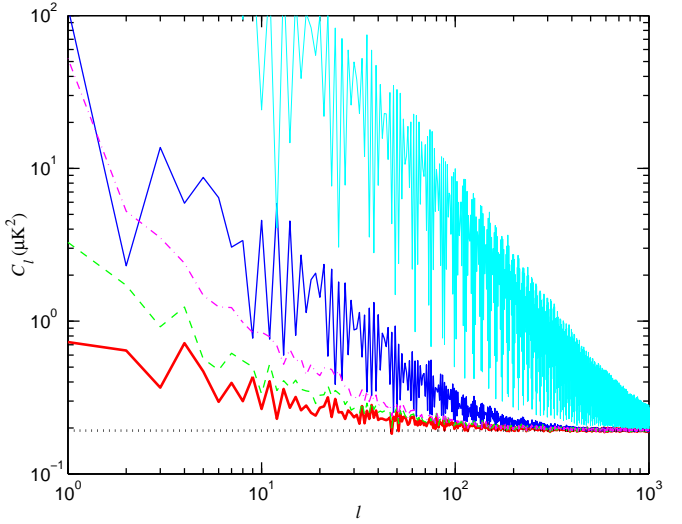


Fig. 8. Same as Fig. 6 but for knee frequency $f_k = 0.025\text{Hz}$.

Looking at the average C_ℓ spectra of residual noise and their std we see that fitting additional base functions decreases the accuracy of destriping at low ℓ . However the situation for the map rms values in Table 3 seems more complicated. For $f_k = 0.1\text{Hz}$ or smaller, fitting additional base functions does not improve the performance of destriping, but with $f_k = 0.4\text{Hz}$ fitting one or two Legendre polynomials besides the constant baselines decreases the map rms, while Fourier components still give inferior results. The improvement in the map rms for $f_k = 0.4\text{Hz}$, when fitting Legendre polynomials, comes from the high multipoles. This can be seen from Fig. 9, where we plot the difference between the residual noise C_ℓ obtained when fitting Legendre polynomials or Fourier components, and when fitting uniform baselines only.

We see that increasing the number of base functions improves the high ℓ but worsens the low ℓ part of the C_ℓ spectra. This is true both for Fourier components and for Legendre polynomials. This trend persists for lower f_k , only that the value of ℓ above which we get an improvement goes up and the improvement for those ℓ becomes smaller.

Delabrouille (1998) obtained improved results by fitting several base functions already with $f_k = 0.1\text{Hz}$. The difference between our results and his is probably due to differences in the noise model. While we assume $P \propto f^{-1}$ as appropriate to LFI radiometers (Seiffert et al. 2002), Delabrouille assumes a noise spectrum of the form $P \propto f^{-2}$ to account also for possible thermal fluctuations and atmospheric noise in ground based and balloon borne bolometer experiments. This leads to more low-frequency noise for a given knee frequency.

The std of the residual noise C_ℓ influences the accuracy at which the C_ℓ spectrum of the CMB can be estimated from the noisy data. From Fig. 10 we can see that at low ℓ uniform baselines give the best performance in the sense that the C_ℓ of the residual noise varies the least

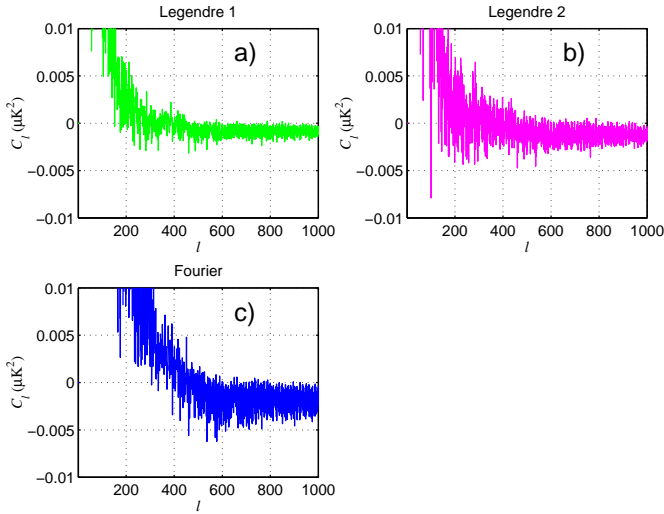


Fig. 9. Differences between C_ℓ spectra shown in Fig. 7 ($f_k = 0.4$ Hz). The three panels show the change in the C_ℓ spectrum when fitting Legendre polynomials up to a) 1st or b) 2nd order, or c) three Fourier components, instead of uniform baselines only.

from one realization to another. At high ℓ there is no clear difference between the performances of different sets of base functions.

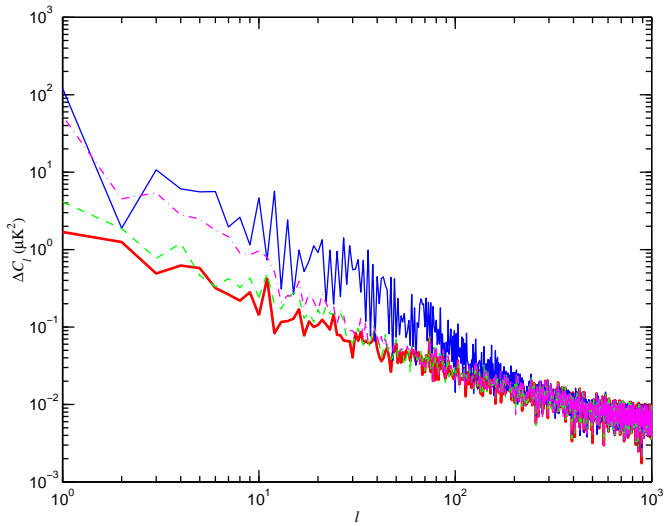


Fig. 10. Standard deviation (std) of the residual noise C_ℓ over 10 noise realizations, for different choices of the base functions. Thick solid (red) line: uniform baselines. Thin solid (blue) line: three Fourier components ($q = 0, 1, 2$). Dashed (green) and dot-dashed (magenta) lines: Legendre polynomials up to 1st and 2nd order. The corresponding map rms and std of map rms values are shown in Table 3 in the middle column ($f_k = 0.1$ Hz).

Table 3. Average rms (upper set) and std of rms (lower set) of the residual noise map (in μ K), for different sets of base functions and for three different knee frequencies. The base functions were: Un: uniform baseline, F1: three Fourier modes, L1 (L2): Legendre polynomials up to 1st (2nd) order. The first line ('Un.') of $f_k = 0.1$ Hz represents the same destriping method as the last line of Table 1. The corresponding C_ℓ spectra are shown in Figs. 8, 6, and 7 and the std of the C_ℓ for $f_k = 0.1$ Hz are shown in Fig. , 10.

fit	0.025Hz	0.1Hz	0.4Hz
Un.	221.943	224.445	234.184
F1	223.113	225.590	235.298
L1	222.031	224.464	233.949
L2	222.143	224.543	233.890
fit	0.025Hz	0.1Hz	0.4Hz
Un.	0.069	0.073	0.107
F1	0.158	0.131	0.275
L1	0.072	0.077	0.117
L2	0.089	0.097	0.162

4. Conclusions

We have presented a maximum-likelihood formulation of the destriping approach to the CMB map making problem, and a rigorous derivation of the destriping algorithm, and we have applied it to the case of the PLANCK mission.

We have formulated the method in matrix form, which allows us to apply the conjugate gradient technique in such a way that we can handle very large data sets.

We have compared the three different destriping methods, the one derived here and the other two already presented in the literature, using simulated PLANCK data (one 100 GHz LFI detector). The differences between these methods can be expressed in terms of a weight function, which varies between methods. This function assigns weights to pixels based on the number of observations falling on that pixel.

We found that our new method provides some improvement to the method used in Burigana et al. (1997) and Maino et al. (1999, 2002). However, it was not better than the method given by Delabrouille (1998), although he gives only a heuristic justification for his weight function. The difference between the latter two methods was very small. That the maximum-likelihood derivation did not lead to the optimal method in practice is due to actual noise properties differing from the idealization used in the derivation. We recommend using either the weight function derived here ($w = 1/n_p$) or the one given by Delabrouille ($w = 1/(n_p - 1)$).

We have tested the possibility of improving the accuracy of destriping by fitting more base functions besides the uniform baseline, but we have found no systematic improvement in the case of instrumental $1/f$ noise. (Fitting several base functions may be more beneficial when removing other types of systematics, i.e. periodic fluctuations induced by thermal instabilities.) The optimal selection of base functions seems to depend on the actual spectrum

of the instrument noise, and on which multipoles one is mainly interested in. However, the great virtue of the de-striping method is its simplicity: it does not require prior information on the noise spectrum. We loose this advantage if we incorporate information on the noise spectrum into the method.

Acknowledgements. This work was supported by the Academy of Finland Antares Space Research Programme grant no. 51433. TP wishes to thank the Väisälä Foundation for financial support. We thank CSC (Finland) and NERSC (U.S.A.) for computational resources. DM and CB warmly thank all the coauthors of our “classical destriping code” and the colleagues that contributed to the related applications. We acknowledge use of the CMBFAST code for computing theoretical CMB C_ℓ spectra, developed by U. Seljak and M. Zaldarriaga. We gratefully acknowledge K. Górska and B. Wandelt for their implementation of the SDE noise generation method. Some of the results in this paper have been derived using the HEALPix package (Górska et al. 1999).

References

Bennett, C., Halpern, M., Hinshaw, G., et al. 2003, ApJ submitted, [[astro-ph/0302207](#)]

Burigana, C., Malaspina, M., Mandolesi, N., et al. 1997, Int. Rep. TeSRE/CNR, 198/1997, November, [[astro-ph/9906360](#)]

Burigana, C., Maino, D., Górski, K.M., et al. 2001, A&A, 373, 345

Challinor, D., Mortlock, D.J., van Leeuwen, F., et al. 2002, MNRAS, 331, 994

Delabrouille, J. 1998, A&ASS, 127, 555

Górski, K.M., Hivon, E., & Wandelt, B.D. 1999, in Proceedings of the MPA/ESO Cosmology Conference "Evolution of Large-Scale Structure", ed. A.J. Banday, R.S. Sheth, & L. Da Costa, PrintPartners Ipskamp, NL, 37, [[astro-ph/9812350](#)]

Maino, D., Burigana, C., Maltoni, M., et al. 1999, A&ASS, 140, 383, [[astro-ph/9906010](#)]

Maino, D., Burigana, C., Górski, K.M., Mandolesi, N., & Bersanelli, M. 2002, A&A, 387, 356, [[astro-ph/0202271](#)]

Mennella, A., Bersanelli, M., Burigana, C., et al. 2002, A&A, 384, 736

Natoli, P., De Gasperis, G., Gheller, C., Vittorio, N. 2001, A&A, 372, 346

Press, W.H., Teukolsky, S.A., Wetterling, W.T., & Flannery, B.P. 1992, Numerical Recipes, 2nd ed. (Cambridge University Press, Cambridge)

Seiffert, M., Mennella, A., Burigana, C., et al. 2002, A&A, 391, 1185

van Leeuwen, F., Challinor, A.D., Mortlock, D.J., et al. 2002, MNRAS, 331, 975